Biosensors and Bioelectronics 137 (2019) 255–262

Contents lists available at ScienceDirect

Biosensors and Bioelectronics

journal homepage: www.elsevier.com/locate/bios

Suspended CNT-Based FET sensor for ultrasensitive and label-free detection of DNA hybridization

Yang Sun[a], Zhisheng Peng[a,b], Huamin Li[c], Ziqun Wang[a], Yanqi Mu[a], Guangping Zhang[a], Shuo Chen[a], Siyu Liu[a,b], Gongtang Wang[a,b], Chundong Liu[a], Lianfeng Sun[b,**], Baoyuan Man[a,***], Cheng Yang[a,d,*]

[a] School of Physics and Electronics, Shandong Normal University, Jinan, 250014, People's Republic of China
[b] CAS Key Laboratory of Nanosystem and Hierarchical Fabrication, National Center for Nanoscience and Technology, Beijing, 100190, People's Republic of China
[c] Department of Electrical Engineering, University at Buffalo North Campus, Buffalo, NY, 14260, USA
[d] Institute of Materials and Clean Energy, Shandong Normal University, Jinan, 250014, People's Republic of China

ARTICLE INFO

Keywords:
DNA sensing
Suspended carbon nanotubes
Filed effective transistor
Transport properties calculation
Ultra-high sensitivity

ABSTRACT

A suspended carbon nanotube (SCNT)-based field effective transistor (SCNT-FET), which was fabricated by utilizing the surface tension of liquid silver to suspend a CNT between two Pd electrodes, was proposed for the detection of DNA hybridization. Benefits from the separation between the CNT and the substrates could be observed; namely, the conductivity of a SCNT-FET was much higher (two orders of magnitude) than that of a FET based on an unsuspended CNT and about 50% sensing surface of CNT was freed from substrate. The Slater-Koster tight-binding method was adopted for geometry optimization and transport property calculation of the SCNT bound with DNA. The result showed that the conductance (G = 1/R) of the SCNT decreased in order with the binding of single-stranded DNA (SSDNA, probe DNA) and double-stranded DNA (DSDNA) and that the ability of DSDNA to weaken the conductivity of the SCNT was several times higher than that of SSDNA. SEM and Raman spectroscopy were used to demonstrate that DNA could be bound successfully onto the SCNT using a 1-pyrenebutanoic acid succinimidyl ester (PBASE) as a linkage. Ultra-high sensitivity detection of DNA [with a limit of detection (LOD) as low as 10 aM] was obtained using such an SCNT-FET, which showed a lower value than that of a previously reported FET DNA biosensor whose sensing materials were in direct contact with the substrate.

1. Introduction

Utilizing DNA information for the diagnosis and treatment of diseases at the molecular level is extremely important for precision medicine. Through the comprehensive analysis of DNA gene sequences, valuable medical information can be obtained, which is beneficial for the early prevention of diseases (Long et al., 2014; Hyslop et al., 2016). Therefore, developing sensitive, selective, and rapid DNA detection techniques is becoming increasingly important. Various detection methodologies, such as electrochemical (Jin et al., 2018; Zhao et al., 2018), surface plasmon resonance (Daems et al., 2018; Fathi et al., 2017), and FET (Di Ventra and Taniguchi, 2016; Ping et al., 2016), have been reported for use in DNA detection. Among them, FET-based sensors are currently being considered as a potential DNA detection tool, due to their advantages such as being label-free, low cost, highly sensitive, and very easy to operate (Sarkar et al., 2014; Schöning.,2006).

FET-based sensors that detect charged molecules via electronic responses generated by the specific interactions of DNA with sensing materials have been demonstrated to have superior sensing performance when compared to other types of sensors. Low-dimensional materials (LDMs), including MoS_2, graphene, and carbon nanotubes, have been extensively studied for use as the sensing material of a FET for DNA detection (Cai et al., 2015; Tran et al., 2016; Khosravi et al., 2017). MoS_2-based FET DNA sensors show superlative detection performance, and the reported lowest LOD reached has been 6 fM (Mei et al., 2018). This was reported to be due to its layered sandwich structure, which imbues this type of sensor with unique capabilities, such as a high on/off current ratio and high flexibility (Lee et al., 2015). Graphene-based FET DNA sensors have also been viewed as highly

* Corresponding author. School of Physics and Electronics, Shandong Normal University, Jinan, 250014, People's Republic of China.
** Corresponding author.
*** Corresponding author.
E-mail addresses: slf@nanoctr.cn (L. Sun), byman@sdnu.edu.cn (B. Man), chengyang@sdnu.edu.cn (C. Yang).

https://doi.org/10.1016/j.bios.2019.04.054
Received 24 March 2019; Received in revised form 13 April 2019; Accepted 29 April 2019
Available online 03 May 2019
0956-5663/

promising candidates for next-generation DNA sensors, due to their single atomic layer structures, leading to a high surface-to-volume ratio and ultra-high carrier mobility. Based on this sensor's capacities, the binding kinetics of DNA hybridization and a LOD in the sub-femtomolar range were obtained (Xu et al., 2017; Gao et al., 2018). Similar to graphene, every atom of a CNT is exposed to the environment due to its barrel-shaped monoatomic structure, making the electronic properties of CNTs very sensitive to charged DNA. Therefore, CNTs have also been widely studied as a sensing material for FET DNA sensors (Kim et al., 2012; Tran, 2016; Khosravi., 2017).

Generally speaking, the sensing material of FETs, regardless of whether they are based on MoS_2, graphene, or carbon nanotubes, is directly contacted with the substrate, which causes several non-ideal behaviors: 1) electrical noise is induced by the changed surface potential along the material, which is caused by the additional carriers trapped from the substrate (Lin et al., 2007); 2) the rough substrate can decrease the mobility of the sensing material, which affects the conductivity of a FET DNA sensor (Katsnelson and Geim, 2008); and 3) part of the sensing area is lost due to the direct attachment of sensing material to the substrate, which dramatically weakens the performance of the FET DNA sensor. Therefore, the advantages of an LDM (a high surface-to-volume ratio and ultra-high carrier mobility) are severely limited in DNA hybridization detection. If the sensing material could be separated from the substrate, it would undoubtedly further improve the sensitivity of a FET DNA sensor.

Thus, we proposed and fabricated an SCNT-FET, which provides an ultra-sensitive platform for DNA hybridization detection. A simple method that utilized the surface tension of liquid silver to suspend a CNT between two Pd electrodes in a high-temperature annealing process was used to fabricate it. The shortcomings of traditional FETs that underutilize the key advantages (high surface-to-volume ratio and ultra-high carrier mobility) of LDM were solved by such a design. A 10 aM LOD for DNA hybridization was obtained, which far exceeds that of other reported FETs. Moreover, to qualitatively verify the experimental results, the Slater-Koster tight-binding method was adopted for geometry optimization and transport properties calculation of CNT bound with DNA, which is rarely studied in current related reports but was necessary for the systematicity and accuracy of our experiments. The successful application of this design opens up new avenues for employing suspended LDMs as the FET sensing material to improve the LOD of DNA hybridization.

2. Experimental section

2.1. Suspended CNTFET fabrication

The specific process of fabricating the SCNT-FET is shown in Fig. S1. Source/drain electrodes (Pd, patterned by using electron-beam lithography) were first deposited on a SiO_2 (800 nm)/Si substrate. The Pd electrodes were deposited by metal evaporation of 3 nm chromium (Cr) as an adhesive layer with 100 nm palladium. The patterned electrodes were then obtained by a lift-off process. Next, a 400-nm-thick silver film was deposited by thermal evaporation, as shown in Fig. S1b. Then, an individual CNT was deposited onto the surface of the Ag film at the deposition zone of the CNT growth furnace as shown in Fig. S1c. The CNTs were obtained by using floating catalytic CVD with 1000 sccm Ar and 10 sccm CH_4 at 1100 °C, and the deposition time used was about 1–2 s to obtain isolated individual CNTs, as reported previously (Zhang et al., 2017). Finally, the devices were placed in a tube furnace to be treated at a high temperature of 961 °C. This was crucial for forcing the liquid silver to move to either side of the Pd electrodes (solid state), straightening the CNT. The specific process of straightening of the CNT was as follows: the device was first heated to 961 °C for 90 min in an atmosphere of 800 sccm Ar and 90 sccm H_2 and then treated at this temperature (961 °C) for 1 min. Finally, the sample was cooled to room temperature. After the above thermal treatment process, the CNT was suspended as shown in Fig. S1d. Palladium and silver are infinitely miscible, which was important for straightening of the CNT.

2.2. Device functionalization

PBASE dissolved in N,N-dimethylformamide was used as the linkage of probe DNA to CNT. Second, 10 mM PBASE is added in channel surface to infiltrate CNT, 1 h later, N,N-dimethylformamide was used to remove extra PBASE. Third, 1 μM 5′-amino modification probe DNA was dropped in channel surface to combine the PBASE, nonbound DNAs were rinsed off with PBS buffer solution. Finally, 100 mM ethanolamine was used to deactivate the excess reactive groups of PBASE and prevent possible nonspecific binding events, then rinsed by DI water. After above, the device have been modified. DNA hybridization was conducted by dropping an appropriate concentration of full-complementary DNA (FCDNA) solution onto the device and incubated for 1 h. To prove specificity, the same procedure was repeated by using the non-complementary DNA sequences instead of the FCDNA sequence to perform the hybridization with the probe DNA. Detailed information about above materials is shown in Fig. S2.

2.3. Characterizations

The electrical properties of the SCNT-FET were determined using a Keithley 4200-SCS semiconductor parameter analyzer and vacuum probing station. Scanning electron microscopy (SEM, Zeiss Gemini Ultra-55) was used to characterize the morphologies of the samples. For accurately distinguishing the subtle changes in the characteristic peaks of CNTs caused by DNA interaction, a 1800 g/mm diffraction grid was used. The laser power was set to 0.5 mW to avoid sample heating and photo-induced damage. The Raman spectroscopy instrument used in this study was a Horiba HR Evolution 800 with laser excitation (532 nm).

3. Results and discussion

A schematic structure of the proposed SCNT-FET is shown in Fig. 1a. It can be clearly observed that the whole surface of the SCNT could be bound with by DNA molecules, which effectively increased the sensing area of the FET compared to that of an unsuspended CNT-FET. To explore the optimal suspended effects on a CNT, a 4*4 mm^2 wafer of substrates designed with four kinds of palladium electrode channels (1.2.3.4μm) was patterned using electron-beam lithography (Fig. S1a). The 100-nm-thick pattered Pd electrodes and 400-nm-thick silver films were deposited in sequence by thermal evaporation (Fig. S1b). A CNT was then deposited and adhered to the surface of the silver substrate (Fig. S1c). Such samples were then heated to 961 °C (the melting point of silver) for 90 min under an Ar/H_2 atmosphere. After thermal treatment for 1 min, partial CNTs broke or sunk and had a channel spacing of 2.3.4μm, as shown in Fig. S1d and the left inset in Fig. 2, but CNTs could be 100% suspended between the Ag/Pd electrodes with a channel length of 1μm as shown in Figs. S1d and 1c.

3.1. Fabrication and electrical properties of suspended CNT-FETs

Silver aggregation to the nearby Pd electrodes and their surface tension on the CNT were the reasons why the CNT could be straightened and suspended (Plateau, 1861). Due to the hydrophobic-like characteristics of silver on a SiO_2 substrate, liquid silver tends to form particle-like shapes to satisfy minimum surface energy when a silver film is heated to its melting point of 961 °C, which was explained by Plateau-Rayleigh instability (Wright et al., 1999). When the silver film in the channel turned into a liquid and was infinitely miscible with Pd (melting point: 1552 °C), a constant force caused by surface tension of 1.67 nN per micrometer was applied to the CNT in the silver motion process (Zhang et al., 2017). Thus, the CNTs were straightened and

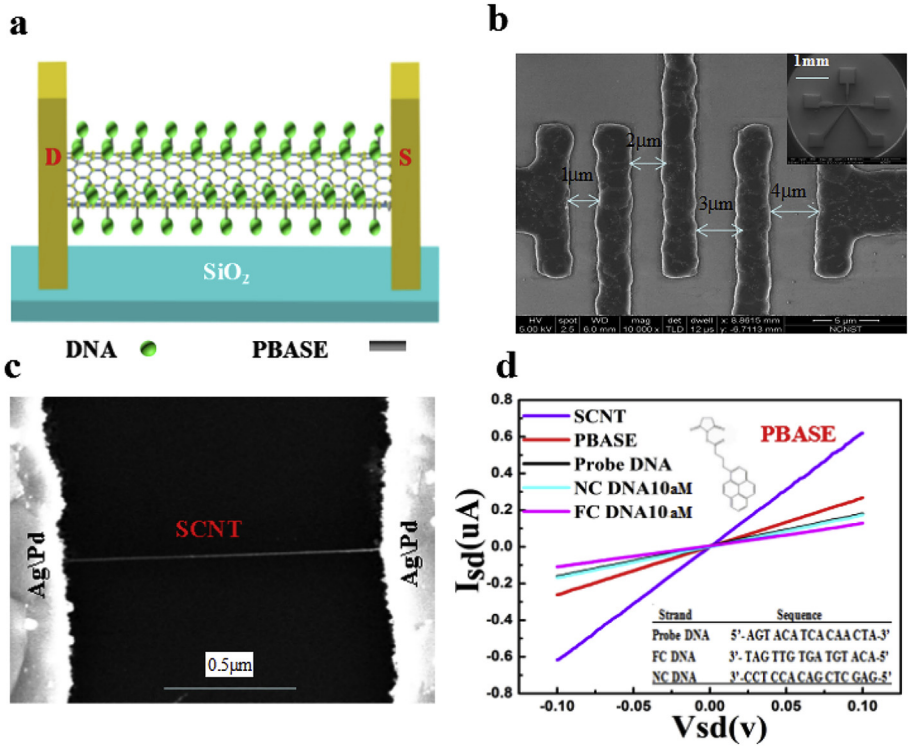

Fig. 1. (a) Schematic of a SCNT-FET. (b) Optical micrograph of the device with 100-nm-thick patterned Pd electrodes. (c) SEM image of an SCNT between two electrodes. (d) Typical I_{sd}-V_{sd} curve of the SCNT-FET device.

suspended in such annealing processes. Such suspended CNTs could be easily formed when the channel spacing was 1μm in our experiments, which is shown in Fig. 1c. We designed four kinds of palladium electrode channels with different lengths (Fig. 2), which all had different suspension effects on CNTs. Longer channel spacing could cause unsatisfactory effects such as sinking or breaking of a CNT (left inset in Fig. 2). This may have been due to the channel being too long or the carbon nanotubes receiving too much force. It is worth mentioning that our method of FET fabrication was transfer-free, which avoids the complex transfer processes used in traditional FET fabrication, as the

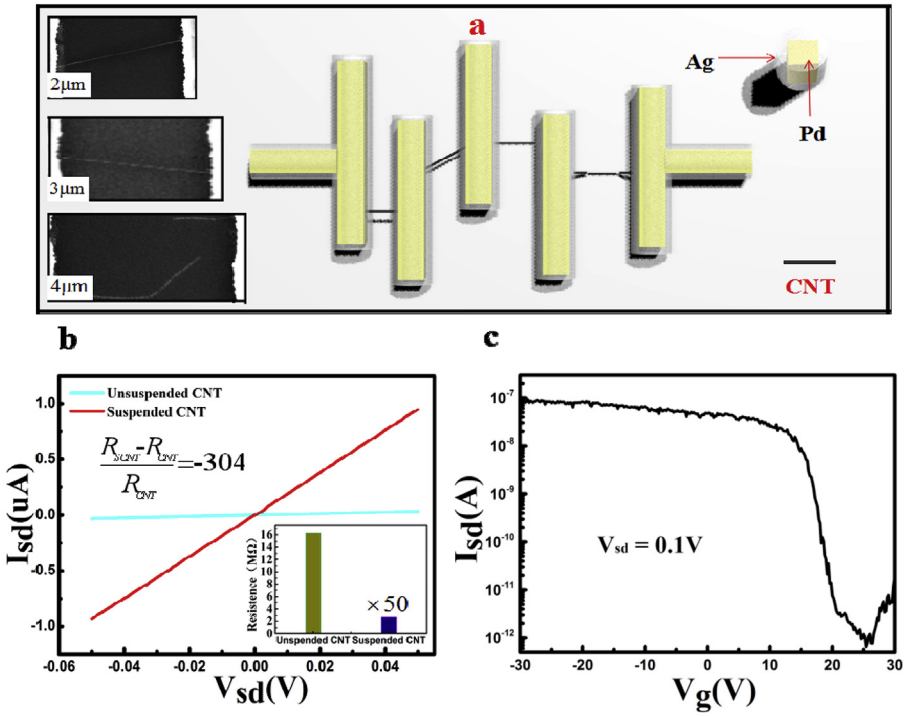

Fig. 2. (a) Schematic of a suspended and an unsuspended CNT. The left inset shows a partially enlarged SEM image of an SCNT-FET with a channel spacing of 2.3.4μm. (b) Comparison of the conductivity between a suspended CNT with an unsuspended CNT. In the inset, × 50 represents that the resistance of suspended CNT is amplified 50 times. (c) I_{sd}-V_g curve of the SCNT FET.

sensing material inevitably becomes damaged and various impurities remain.

Eliminating the adverse effect of a substrate on a CNT is extraordinarily effective for improving the electrical performance of a CNT. Significant changes in the conductivity of a suspended or unsuspended CNT were easily observed, as shown in Fig. 2b. The slope of a typical source-drain current (I_{sd}) versus voltage (V_{sd}) characteristic curve exhibited great difference, and the resistance of such an SCNT was reduced by two orders of magnitude compared to an unsuspended CNT (inset in Fig. 2b). The FET transfer characteristics in Fig. 2c suggested that the SCNT was a p-type semiconductor, which indicated that the main carrier in the CNT was its hole. Similar to fabricated p-type graphene, the negative effect of the substrate was mainly due to its donating electrons (Wang et al., 2012). The trapping and detrapping of carriers change the number of local carriers along a CNT and also vary the surface potential along it. In addition, the roughness of a substrate can introduce short-range scattering centers that cause the decrease in mobility in CNTs (Lin et al., 2007; Katsnelson and Geim, 2008).

3.2. Functionalization and hybridization of SCNT-FET

The detailed process of probe DNA immobilization and target DNA hybridization is shown in Fig. 3. PBASE dissolved in N,N-dimethylformamide was used as the linkage to ensure the probe DNA could be successfully bound to an SCNT and avoid introducing defects (caused by covalent interaction) to a SCNT as shown in Fig. 3a (Wang et al., 2012; Khosravi et al., 2017). As shown in Fig. 3b, PBASE binds to an SCNT through π stacking (non-covalent interaction) of its pyrene group onto the SCNT surface. The succinimide portion of PBASE extends out from the SCNT surface and permits immobilization of 5′-amine-modified probe DNAs through a conjugation reaction between the amine group of the probe DNA and the amine-reactive succinimide group of PBASE, as shown in Fig. 3c. Finally, to prevent nonspecific adsorption, ethanolamine was used as a blocking agent, as its tail end amino groups can work as a blocking agent and react with excess PBASE termini (Fig. S3). After the above steps, complementary DNAs were added to hybridize with the probe DNAs through base pairing. At each step of the experiment, the sample was dried in a dry box at 40 °C (DNA be inactivated above 90 °C), and the detection of I_d-V_d proceeded after it had dried.

3.3. Characterization of suspended CNT-FETs after functionalization and hybridization

For demonstrating such SCNT-FETs can successfully work as a DNA sensor, it was necessary to demonstrate that the SCNT could effectively bind to DNA and that the SCNT did not break or sink during detection. A DNA bound or unbound SCNT was thus characterized by Raman spectroscopy and SEM. In the SEM image of a bare SCNT with a diameter of about 10 nm, the surface was smooth and without attachment (Fig. 4a). After DNA hybridization, the surface of the SCNT became uneven and was wrapped with layers of attachments, and the diameter also changed to 13–18 nm as shown in Fig. 4b. To demonstrate that the attachment was DNA, we characterized it using Raman spectroscopy. Compared to that of a bare SCNT, Raman spectroscopy of an SCNT bound with DNA displayed more characteristic peaks in the low-frequency regions (Fig. 4c), which could be readily assigned to PBASE and DNA. The peak at 1337.2 cm^{-1} was from sp^3 bonding. The peak at 1615.4 cm^{-1} could be assigned to pyrene group resonance, and the peak at 1361.7 cm^{-1} was due to the introduction of disorder arising from orbital hybridization of the molecule with the CNT surface. The peaks at 122.16 cm^{-1}, 1415.8 cm^{-1}, and 1687.9 cm^{-1} were attributed to the addition of probe DNA and target DNA, which was in agreement with published results (Xu et al., 2017) and more information which proves that the attachments were DNA was added in section A in supplementary materials. Compared to a broken or sunken CNT caused by the fabrication process (Fig. 4d), the SEM image of an SCNT bound with DNA shows that the CNT was still suspended and not broken or sunken, as shown in Fig. 4b.

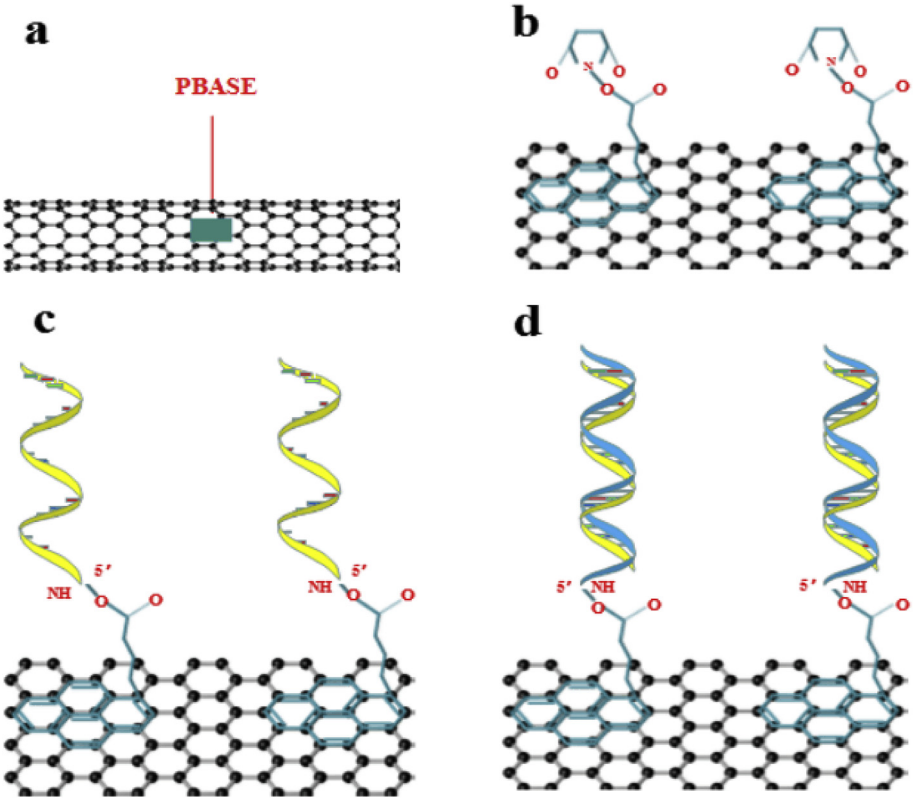

Fig. 3. Schematic illustration of a suspended CNTFET for DNA detection. (a) Functionalization of the SCNT surface by PBASE. (b) Schematic of PBASE interacting with an SCNT. (c) PBASE interacting with probe DNA to achieve probe DNA binding to an SCNT. (d) Probe DNA interacting with FC DNA to form double-stranded DNA.

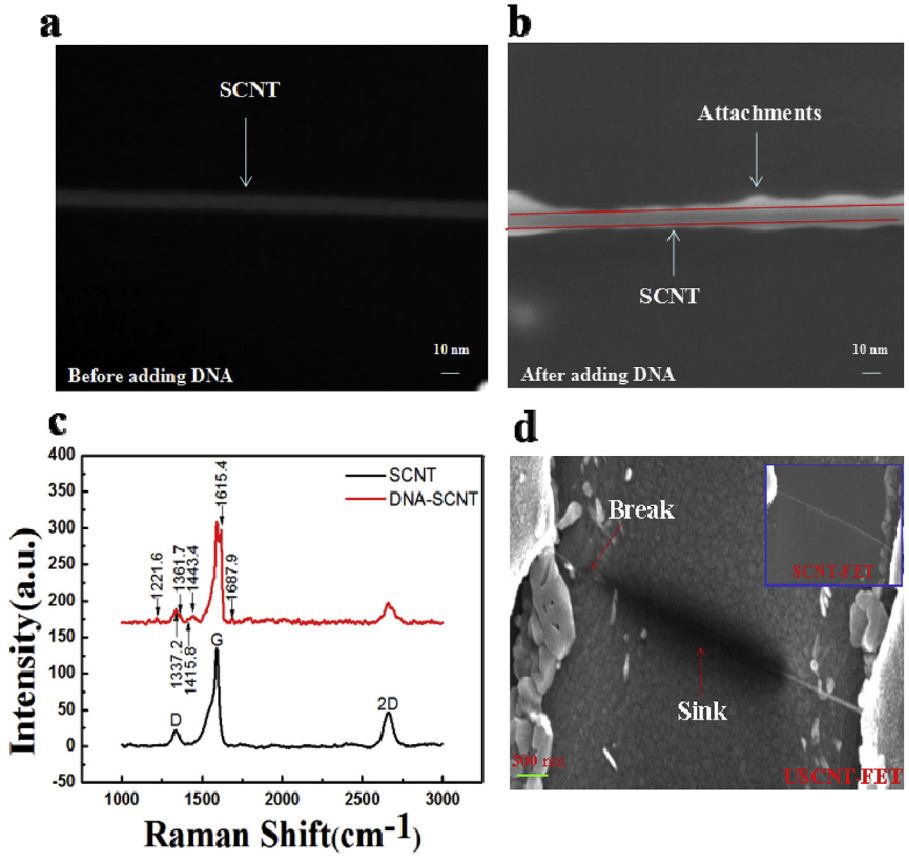

Fig. 4. (a) SEM image of suspended carbon nanotubes combined without any substance. (b) SEM image of suspended carbon nanotubes after completing DNA binding and hybridization. (c) Raman spectra of an SCNT before and after the completion of functionalization and hybridization. (d) SEM image of a sunk or broken CNT.

3.4. Sensitivity

From Figs. 5a and 1d, it can be seen that the LOD of an SCNT-FET reached 10 aM and the sensor showed good specificity, proving that it could perform DNA detection. The slope of the V_{sd}-I_{sd} curves became smaller in turn after adding PBASE, probe DNA, and FCDNA. In

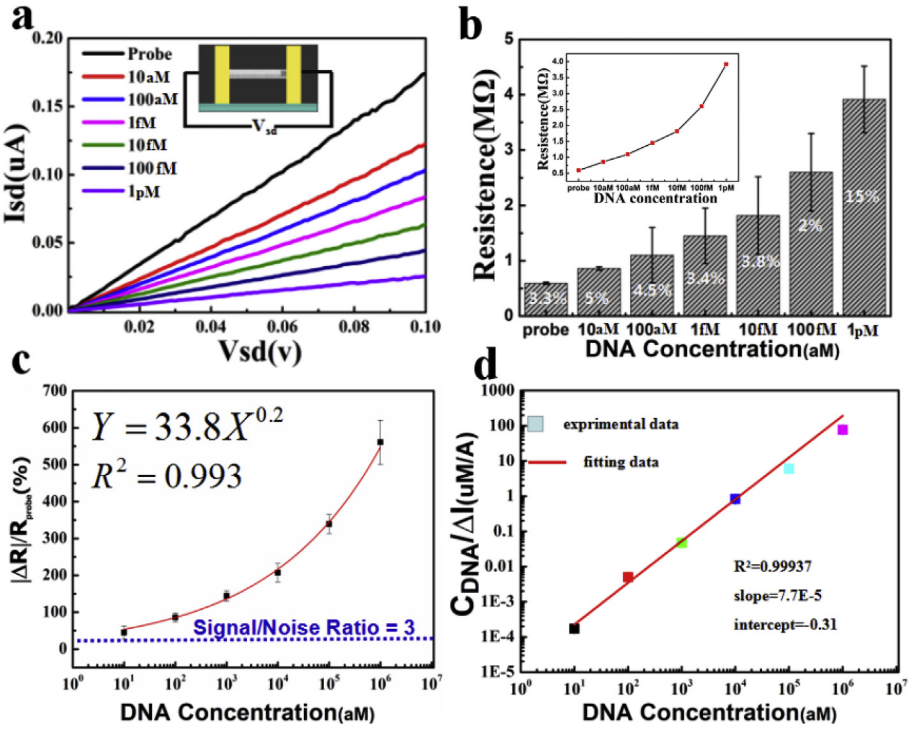

Fig. 5. (a) I_{sd}-V_{sd} curve of an SCNT-FET device hybridized with FC-DNA at a series of concentrations from 10 aM to 1 pM (V_{sd} from 0 to 0.1 V; V_g = 0 V). (b) The resistances of SCNT to DNA hybridization detection at different concentrations. (c) The calibration curve for the detection of DNA. Dashed line represents a triple noise level (~22.5%) from a blank control test. (d) DNA concentration (C_{DNA})/the amount of net drain current (ΔI) was plotted as a function of C_{DNA}.

contrast, only small differences were observed after adding NC DNA, and the lake blue line almost coincided with the black line, suggesting that an SCNT-FET is highly specific as shown in Fig. 1d (Xu et al., 2017; Kim et al., 2012). The sensitivity and the linear relationship were investigated by determining the hybridization of FCDNA with probe DNA (Fig. 5a and c). We observed that the slope of the I_{sd}-V_{sd} curve was significantly decreased with the addition of increased concentrations of target DNA (from 10 aM to 1 pM). The changes in resistance, corresponding to the I_{sd}-V_{sd} curve, are shown in Fig. 5b, where the error bars and the relative standard deviations (RSD) suggest that the device had good repeatability. The linear relationship of $\Delta_{resistance}$ was represented by $\Delta R/R_{probe}$ (%) = 33.8 $C_{DNA}{}^{0.2}$ (aM) (R^2 = 0.99397), which clearly showed that as the concentration of DNA increased, the resistance increased exponentially, similar to previous publications (Kim et al., 2012), as shown in Fig. 5c. Note that the concentration of DNA at 1 aM was also tested. As previous article reported (Mei et al., 2018), the detection signal of the lowest concentration of target DNA must be higher than the noise signal to be considered valid. However, the detected signal of DNA at 1 aM was lower than the noise level (22.5%), so the data about DNA with a concentration of 1 aM were not valid and could not be placed in Fig. 5a and c. The concentration of DNA as low as 10 aM was determined based on a signal level (45%) that exceeded the background by threefold (noise level 22.5%). The above results demonstrate that the LOD of such an SCNT-FET sensor should be approximately 10 aM. To further demonstrate that the SCNT-FET could effectively detect DNA at such a low concentration, the affinity of the reaction between probe DNA and target DNA was investigated. DNA concentration (C_{DNA})/the amount of net drain current (ΔI) was plotted as a function of C_{DNA}, as shown in Fig. 5d. From the results (Fig. S4), we know that the adsorption of target DNA onto probe DNA on CNT channels followed the Langmuir adsorption isotherm, which is given by (Abe et al., 2007; Maehashi et al., 2009)

$$\frac{C_{DNA}}{\Delta I} = \frac{C_{DNA}}{\Delta I_{sat}} + \frac{K_d}{\Delta I_{sat}} \quad (1)$$

where K_d is the dissociation constant of the reaction between probe DNA and target DNA, and ΔI_{sat} is the amount of saturated drain current. From curve fitting, the dissociation constant was estimated to be 4.03×10^{-9} M. The value of K_d was almost identical to reported results (Su et al., 2018; Esteban Fernandez de Avila et al., 2013; Park et al., 2006), which demonstrates that there was a fine affinity between the target DNA and probe DNA, and that the DNA at such a low concentration could be effectively detected by the SCNT-FET.

3.5. Theoretical simulation

In order to qualitatively verify our conclusions, theoretical calculations were performed, of which the common tendency accords well with our experimental result. Fig. 6 depicts the model constructed based on a CNT covered by DADNA. The models of a pristine CNT device (CNT) and a SSDNA CNT covered device are shown in Figs. S5 and S6. Three models were designed with reference to the reported articles about molecular dynamics simulation (Roxbury et al., 2012; Johnson et al., 2009). The model could be divided into three parts: the semi-infinite left electrode, the central region, and the semi-infinite right electrode. The structural optimization and electrical transport properties were calculated using the Atomistix ToolKit (ATK) package. Limited by computational resource, it was impossible to perform the calculations for such huge numbers of atoms using the density functional theory (DFT). Hence, SSDNA was simplified as a single base, and DSDNA was simplified as two bases that were complementary to each other, and the Slater-Koster tight-binding method was adopted for geometry optimization and the following transport properties calculations. Basis sets were selected as CP2K, and the residue force on every atom was less than 0.05 eV/Å. Transport properties were calculated by using the nonequilibrium Green's method, combined with a tight-bind DFT. A 1×1×100 mesh was used for the k-point sampling in the Brillouin zone (BZ), and the convergence criterion for the Hamiltonian matrix was chosen as 10^{-4} Hartree. As shown in Fig. 6 and S5-S7, the depth of the valley peak in the transmission spectra represented the degree of weakening in the CNT conductivity. For CNT, the transmission coefficient was always equal to 2 in the range [-0.5 eV, 0.5 eV] except at Fermi Energy (Fig. S5), which originates from the twofold degenerate energy bands. The conductance (G = 1/R) of a bare CNT decreased in order from $G_{CNT} > G_{CNT+SSDNA} > G_{CNT+DSDNA}$ with the addition of SSDNA and DSDNA, and the ability of DSDNA to weaken the conductivity of a CNT was more than twice (at least 5–6 times or even higher) than that of SSDNA. The above results were deduced from the following three points. First, from Figs. S6 and S7, we know that there were new valley peaks that appeared at 3 and 4 after adding FCDNA, which was due to DNA hybridization. After careful observation, we found that the depth of the valley peaks at 3 was almost equal to that at 2 and that the depth of valley peaks at 4 was deeper (more than twofold) than that at 1, which suggested that the additional factors caused by hybridization had almost the same ability to weaken the resistance of a CNT as that of single-stranded DNA. Second, the peaks in the wireframes marked A and B (top right in Fig. 6) show that the valley peaks caused by DSDNA (blue line) were much deeper (~three times at 5 and ~five times at 6) than that caused by ssDNA (red line), which was consistent with experimental results. Third, the location of valley peaks caused by SSDNA moved toward the Fermi energy after adding FCDNA, which suggested the conductivity was further weakened (top right in Fig. 6; after adding FCDNA, the red line moved to blue line). The above simulation results fully explain the experimental results that the resistance of a CNT + Probe DNA decreased with the addition of FCDNA and that the variation in the resistance of a CNT + PBASE caused by the FCDNA was much larger than that caused by probe DNA, consistent with previous reports (Figs. 5b and 1d).

The improvement in LOD of the DNA hybridization is the focus studied by many groups, as shown in Table S1. As observed, the suspended SCNT-FET biosensor developed in this work exhibited the highest sensitivity (10 aM). We believe that there were two mechanisms for this phenomenon. First, the local carrier concentration and mobility of the CNT were mainly affected by doping effects (charge transfer) caused by the substrate or adsorbed molecules. Electron donation from the probe DNA, target DNA, or the charged molecules trapped on the substrate resulted in a decrease in the charge carrier concentration of the p-type SCNT, which leads to step-like changes in resistance. Second, the local carrier concentration and mobility of a CNT are also affected by the scattering effect of absorbs or substrate, which introduces short-range scattering centers. For the case of a suspended CNT that was separated from substrate, there were no substances that could lead to doping effects or scattering effects on the CNT except for DNA. So the purity of detected signal was enhanced. Also, an SCNT-FET significantly improved the sensing area and conductivity, which accelerated the signal transmission. The combination of the above advantages enables it to possess extremely high detection performance.

4. Conclusion

We developed an SCNT-FET sensor for DNA hybridization detection. Such sensors successfully avoid the adverse effects of a substrate on a sensing material and have a larger sensing area, better conductance, and purer electrical signals than those with a traditional FET sensor. DNA can bind well to a suspended CNT, which was not broken during detection. A detection limit up to 10 aM was obtained by using such an SCNT-FET sensor. Theoretical simulations show that the conductance (G = 1/R) of a CNT decreased in the order $G_{CNT} > G_{CNT+SSDNA} > G_{CNT+DSDNA}$, and the ability of dsDNA to weaken the conductivity of a CNT was several times higher than that of ssDNA. The combination of experiment and theoretical simulation demonstrated that an SCNT-FET could be used as an effective DNA sensor.

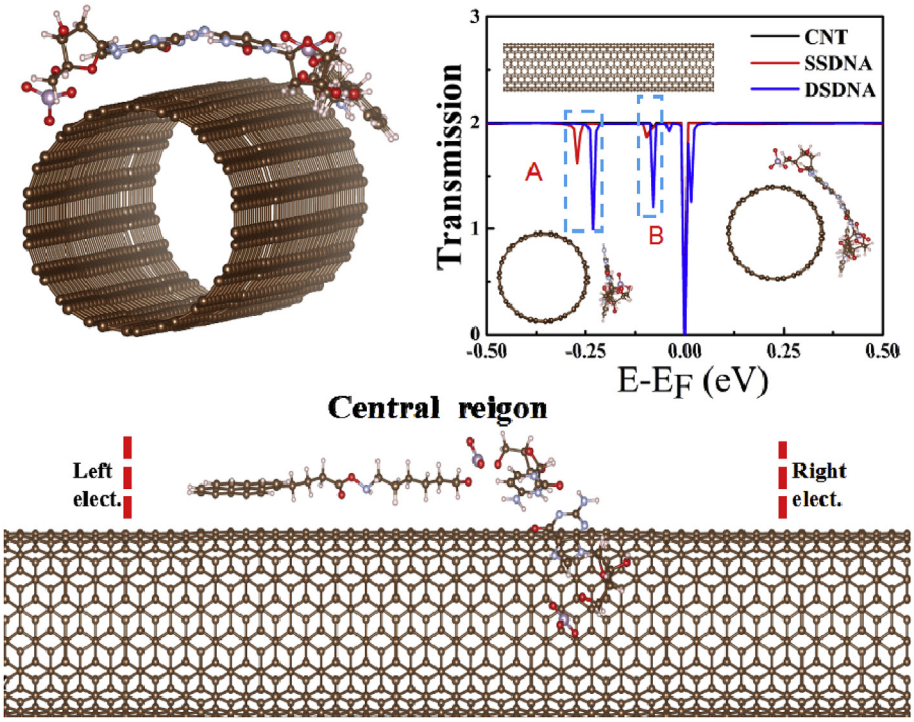

Fig. 6. A model constructed based on a CNT covered by double-stranded DNA and the calculated transmission spectrum.

Here, gate-controlled FET was not formed due to the small size of a suspended CNT, and the effects of the gate voltage were not analyzed. In the future, we will investigate a moderate DNA reaction vessel to form a liquid-gate FET DNA sensor. We believed that using suspended graphene or TMDCs (such as MoS_2) or their heterostructures as the sensing materials will further improve the sensitivity.

Declaration of interests

☒ The authors declare that they have no known competing financial interests or personal relationships that could have appeared to influence the work reported in this paper.

☐The authors declare the following financial interests/personal relationships which may be considered as potential competing interests:

CRediT authorship contribution statement

Yang Sun: Conceptualization, Methodology, Software, Validation, Formal analysis, Investigation, Resources, Data curation, Writing - original draft, Visualization. **Zhisheng Peng:** Methodology, Investigation. **Huamin Li:** Formal analysis, Writing - review & editing. **Ziqun Wang:** Software. **Yanqi Mu:** Software. **Guangping Zhang:** Software, Formal analysis, Resources. **Shuo Chen:** Validation. **Siyu Liu:** Methodology. **Gongtang Wang:** Validation, Resources, Writing - review & editing. **Chundong Liu:** Data curation. **Lianfeng Sun:** Methodology, Resources, Writing - review & editing. **Baoyuan Man:** Conceptualization, Writing - review & editing, Supervision. **Cheng Yang:** Conceptualization, Formal analysis, Resources, Data curation, Writing - review & editing, Supervision, Project administration, Funding acquisition.

Acknowledgments

The authors are grateful for financial support from the National Natural Science Foundation of China (11874244, 11774208 and 11474187) and Shandong Provincial Natural Science Foundation, China (ZR2016AM19).

Appendix A. Supplementary data

Supplementary data to this article can be found online at https://doi.org/10.1016/j.bios.2019.04.054.

References

Abe, M., Murata, K., Kojima, A., Ifuku, Y., Shimizu, M., Ataka, T., Matsumoto, K., 2007. Quantitative detection of protein using a top-gate carbon nanotube field effect transistor. J. Phys. Chem. C 111 (24), 8667–8670.

Cai, B., Huang, L., Zhang, H., Sun, Z., Zhang, Z., Zhang, G.-J., 2015. Gold nanoparticles-decorated graphene field-effect transistor biosensor for femtomolar MicroRNA detection. Biosens. Bioelectron. 74, 329–334.

Daems, D., Pfeifer, W., Rutten, I., Sacca, B., Spasic, D., Lammertyn, J., 2018. 3D DNA origami as programmable anchoring points for bioreceptors in fiber optic surface plasmon resonance biosensing. ACS Appl. Mater. Interfaces 10 (28), 23539–23547.

Di Ventra, M., Taniguchi, M., 2016. Decoding DNA, RNA and peptides with quantum tunnelling. Nat. Nanotechnol. 11 (2), 117.

Esteban Fernandez de Avila, B., Watkins, H.M., Pingarrón, J.M., Plaxco, K.W., Palleschi, G., Ricci, F., 2013. Determinants of the detection limit and specificity of surface-based biosensors. Anal. Chim. 85 (14), 6593–6597.

Fathi, F., Rezabakhsh, A., Rahbarghazi, R., Rashidi, M.-R., 2017. Early-stage detection of VE-cadherin during endothelial differentiation of human mesenchymal stem cells using SPR biosensor. Biosens. Bioelectron. 96, 358–366.

Gao, Z., Xia, H., Zauberman, J., Tomaiuolo, M., Ping, J., Zhang, Q., Ducos, P., Ye, H., Wang, S., Yang, X., 2018. Detection of Sub-fM DNA with Target Recycling and Self-Assembly Amplification on Graphene Field Effect Biosensors.

Jin, X., Zhou, L., Zhu, B., Jiang, X., Zhu, N., 2018. Silver-dendrimer nanocomposites as oligonucleotide labels for electrochemical stripping detection of DNA hybridization. Biosens. Bioelectron. 107, 237–243.

Johnson, R.R., Kohlmeyer, A., Johnson, A.C., Klein, M.L., 2009. Free energy landscape of a DNA− carbon nanotube hybrid using replica exchange molecular dynamics. Nano Lett. (2), 537–541.

Katsnelson, M., Geim, A., 2008. Electron scattering on microscopic corrugations in graphene. Phil. Trans. Roy. Soc. Lond.: Math. Phys. Eng. Sci. 366 (1863), 195–204.

Khosravi, F., Loeian, S., Panchapakesan, B., 2017. Ultrasensitive label-free sensing of IL-6 based on PASE functionalized carbon nanotube micro-arrays with RNA-aptamers as molecular recognition elements. Biosensors 7 (2), 17.

Kim, B., Lee, J., Namgung, S., Kim, J., Park, J.Y., Lee, M.-S., Hong, S., 2012. DNA sensors based on CNT-FET with floating electrodes. Sensor. Actuatb-Chem 169, 182–187.

Lee, D.-W., Lee, J., Sohn, I.Y., Kim, B.-Y., Son, Y.M., Bark, H., Jung, J., Choi, M., Kim, T.H., Lee, C., 2015. Field-effect transistor with a chemically synthesized MoS_2 sensing channel for label-free and highly sensitive electrical detection of DNA hybridization. Nano. Res. 8 (7), 2340–2350.

Lin, Y.-M., Tsang, J.C., Freitag, M., Avouris, P., 2007. Impact of oxide substrate on electrical and optical properties of carbon nanotube devices. Nanotechnology 18

(29), 295202.
Long, C., McAnally, J.R., Shelton, J.M., Mireault, A.A., Bassel-Duby, R., Olson, E.N., 2014. Prevention of muscular dystrophy in mice by CRISPR/Cas9–mediated editing of germline DNA. Science 345 (6201), 1184–1188.
Maehashi, K., Matsumoto, K., Takamura, Y., Tamiya, E., 2009. Aptamer-based label-free immunosensors using carbon nanotube field-effect transistors. Electroanalysis: Int. J. Dev. Fund. Pract. Asp. Electroanal. 21 (11), 1285–1290.
Mei, J., Li, Y.-T., Zhang, H., Xiao, M.-M., Ning, Y., Zhang, Z.-Y., Zhang, G.-J., 2018. Molybdenum disulfide field-effect transistor biosensor for ultrasensitive detection of DNA by employing morpholino as probe. Biosens. Bioelectron. 110, 71–77.
Park, H., Germini, A., Sforza, S., Corradini, R., Marchelli, R., Knoll, W., 2006. Kinetic and affinity analyses of hybridization reactions between peptide nucleic acid probes and DNA targets using surface plasmon field-enhanced fluorescence spectroscopy. Biointerphases 1 (4), 113–122.
Ping, J., Vishnubhotla, R., Vrudhula, A., Johnson, A.C., 2016. Scalable production of high-sensitivity, label-free DNA biosensors based on back-gated graphene field effect transistors. ACS Nano 10 (9), 8700–8704.
Plateau, M., 1861. XXXVII. Experimental and theoretical researches on the Fig.s of equilibrium of a liquid mass devoid of weight. Fifth Ser. London, Edinburgh Dublin Philosoph. Magaz. J. Sci. 22 (147), 286–293.
Roxbury, D., Mittal, J., Jagota, A., 2012. Molecular-basis of single-walled carbon nanotube recognition by single-stranded DNA. Nano Lett. 12 (3), 1464–1469.
Sarkar, D., Liu, W., Xie, X., Anselmo, A.C., Mitragotri, S., Banerjee, K., 2014. MoS_2 field-effect transistor for next-generation label-free biosensors. ACS Nano 8 (4), 3992–4003.
Su, Q., Vogt, S., Nöll, G., 2018. Langmuir analysis of the binding affinity and kinetics for surface tethered duplex DNA and a ligand–apoprotein complex. Langmuir 34 (49), 14738–14748.
Tran, T.-T., Mulchandani, A., 2016. Carbon nanotubes and graphene nano field-effect transistor-based biosensors. Trac. Trends Anal. Chem. 79, 222–232.
Wang, Q.H., Jin, Z., Kim, K.K., Hilmer, A.J., Paulus, G.L., Shih, C.-J., Ham, M.-H., Sanchez-Yamagishi, J.D., Watanabe, K., Taniguchi, T., 2012. Understanding and controlling the substrate effect on graphene electron-transfer chemistry via reactivity imprint lithography. Nat. Chem. 4 (9), 724.
Wright, D., York, A.E., Coleman, K., Green, M.H., Hutchison, J., 1999. Capillarity and silver nanowire formation observed in single walled carbon nanotubes. Chem. Commun. (8), 699–700.
Xu, S., Zhan, J., Man, B., Jiang, S., Yue, W., Gao, S., Guo, C., Liu, H., Li, Z., Wang, J., 2017. Real-time reliable determination of binding kinetics of DNA hybridization using a multi-channel graphene biosensor. Nat. Commun. 8, 14902.
Zhang, J., Liu, S., Nshimiyimana, J.P., Deng, Y., Hou, G., Chi, X., Hu, X., Zhang, Z., Wu, P., Wang, G., 2017. Wafer-scale fabrication of suspended single-walled carbon nanotube Arrays by silver liquid dynamics. Small 13 (40), 1701218.
Zhao, J., Gao, J., Zheng, T., Yang, Z., Chai, Y., Chen, S., Yuan, R., Xu, W., 2018. Highly sensitive electrochemical assay for Nosema bombycis gene DNA PTP1 via conformational switch of DNA nanostructures regulated by H+ from LAMP. Biosens. Bioelectron. 106, 186–192.